# Fusion of IRST and Radar Measurements for 3D Target Tracking

V P S Naidu, *Member*

*Two different types of measurement fusion methods for fusing IRST (infrared search and track) and radar measurements to track a target in 3D Cartesian coordinates are evaluated and discussed in this paper. Performance evaluation metrics were provided to evaluate the tracking algorithm. It was observed that both the fusion algorithms are performed alike. Proof was provided to show that both the methods are functionally similar.*

***Keywords*** **:** IRST; Radar measurement; Target tracking

## NOTATION

$F$ : state transition matrix

$G$ : process noise gain matrix

$H(k)$ : linearized measurement matrix at time index $k$

$K(k)$ : Kalman gain at time index $k$

$\hat{P}$ : estimated state error covariance matrix

$\tilde{P}$ : predicted state error covariance matrix

$Q$ : process noise covariance matrix

$r_m$ : range, m

$R^{ir}$ : IRST measurement noise covariance matrix

$R^{rd}$ : radar measurement noise covariance matrix

$S$ : innovation covariance matrix

$v(k)$ : measurement noise at time index $k$

$w(k)$ : process noise at time index $k$

$\hat{X}$ : estimated state vector

$\tilde{X}$ : predicted state vector

$z_m{}^{ir}(k)$ : IRST measurement at time index $k$

$z_m{}^{rd}(k)$ : radar measurement at time index $k$

$\tilde{z}$ : predicted measurement

AE : absolute error

MAE : mean absolute error

MVF : measurement vector fusion

NEES : normalized estimation error square

NIS : normalized innovation square

PFE : percentage fit error

RMSE : root mean square error

RSSE : root sum square error

$\varphi_m$ : elevation in radiance

$\theta_m$ : azimuth in radiance

**V P S Naidu is with the Multi Sensor Data Fusion Lab, Flight Mechanics and Control Division, National Aerospace Laboratories, Bangalore 560 017.**

This paper was received on May 19, 2008. Written discussion on the paper will be entertained till July 31, 2009.

## INTRODUCTION

Modern fighter aircraft are well equipped with variety of sensors in order to assist the pilot. If these sensors are perfect, then the target tracking could be achieved by simple geometry. In reality, sensors are not perfect and their measurements are corrupted with noise. Moreover, single sensor may not provide all information about the target. Hence, tracking filters and multi-sensors are used to increase the target tracking capabilities. Generally, radar and infrared search and track (IRST) sensor are used in cockpit for providing target information. Radar can measure azimuth, elevation and range to a target. It can measure range with good resolution, but the angular measurements with good resolution are not possible. Radar provides sufficient information to track the target, since, it measures both angular and range to a target. The uncertainty associated with radar might be represented as a volume whose dimensions are relatively large perpendicular to the measured line of sight and small along the line of sight. An IRST sensor can measure azimuth and elevation of a target with good resolution. It can provide only the direction to a target but not its location because it does not provide the range. The uncertainty associated with IRST might be represented as a square whose dimensions are comparatively small perpendicular to the measured line of sight. From fusion of radar and IRST measurements, it has been observed that the resultant uncertainty of the estimated position of the target is smaller than the uncertainty of the either measurements alone[1-3].

This paper deals with tracking of target in 3D Cartesian coordinates using the measurements from radar and IRST in polar coordinates. 3D target tracking with IRST and radar

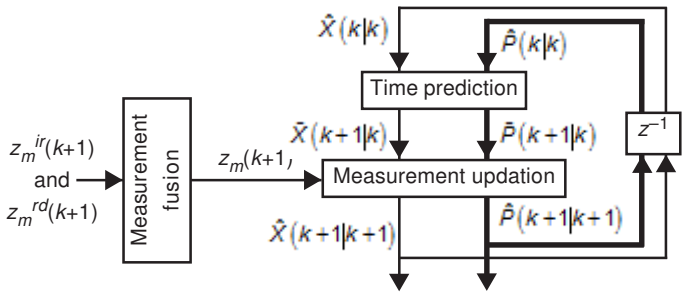


**Figure 1 Information flow diagram measurement fusion and tracking**

measurements can be achieved either by state vector fusion or measurement fusion. In this paper, two measurement fusion methods are presented and evaluated with simulated data. In first method (MVF1), the measurements from IRST and radar are merged into an augmented measurement vector and in the second method (MVF2), the measurements from IRST and radar are combined by using minimum mean square estimates[4]. Extended Kalman filter is used to estimate the state of a target using target motion and measurement models[5]. The performance of tracking algorithms are evaluated in terms of percentage of fit error (PFE), mean absolute error (MAE), root mean square error (RMSE), root sum square error (RSSE), normalized estimation error square (NEES) and normalized innovation square (NIS).

## MEASUREMENT FUSION

The two different measurement fusion algorithms are described here. The information flow diagram is shown in Figure 1.

### MVF1

In this technique, the measurement vectors $z_m^{ir}(k)$ and $z_m^{rd}(k)$ from the IRST and radar, respectively, are merged into an augmented measurement vector as

$$z_m(k) = \begin{bmatrix} z_m^{ir}(k) \\ z_m^{rd}(k) \end{bmatrix} \tag{1}$$

where

$$z_m^{ir}(k) = \begin{bmatrix} \theta_m^{ir}(k) & \varphi_m^{ir}(k) \end{bmatrix}^T$$

and

$$z_m^{rd}(k) = \begin{bmatrix} \theta_m^{rd}(k) & \varphi_m^{rd}(k) & r_m^{rd}(k) \end{bmatrix}^T$$

Similarly, the observation matrices of IRST and radar are merged into an augmented observation matrix as:

$$h(X(k)) = \begin{bmatrix} h^{ir}(X(k)) \\ h^{rd}(X(k)) \end{bmatrix} \tag{2}$$

The measurement noise covariance matrix of IRST and radar are merged as:

$$R = \begin{bmatrix} R^{ir} & 0 \\ 0 & R^{rd} \end{bmatrix} \tag{3}$$

where

$$R^{ir} = \begin{bmatrix} (\sigma_\theta^{ir})^2 & 0 \\ 0 & (\sigma_\varphi^{ir})^2 \end{bmatrix}$$

and

$$R^{rd} = \begin{bmatrix} (\sigma_\theta^{rd})^2 & 0 & 0 \\ 0 & (\sigma_\varphi^{rd})^2 & 0 \\ 0 & 0 & (\sigma_r^{rd})^2 \end{bmatrix}$$

### MVF2

In this technique, weighted combination of measurements based on minimum mean square estimation is considered. The fused measurement vector is computed as:

$$z_m(k) = \frac{c_1 z_m^{ir}(k) + c_2 z_m^{rd}(k)}{c_1 + c_2} \tag{4}$$

where $c_1$ and $c_2$ are the weights.

The weights in equation (4) are computed from the measurement noise covariance matrix as:

$$c_1 = \frac{1}{R^{ir}} \text{ and } c_2 = \frac{1}{R^{rd}} \tag{5}$$

$$z_m(k) = \frac{\frac{1}{R^{ir}} z_m^{ir}(k) + \frac{1}{R^{rd}} z_m^{rd}(k)}{\frac{1}{R^{ir}} + \frac{1}{R^{rd}}}$$

The final form of measurement fused vector is:

$$z_m(k) = \frac{R^{rd} z_m^{ir}(k) + R^{ir} z_m^{rd}(k)}{R^{ir} + R^{rd}}$$

or

$$z_m(k) = \frac{R^{rd} z_m^{ir}(k)}{R^{ir} + R^{rd}} + \frac{R^{ir} z_m^{rd}(k)}{R^{ir} + R^{rd}} + \frac{R^{ir} z_m^{ir}(k)}{R^{ir} + R^{rd}} - \frac{R^{ir} z_m^{ir}(k)}{R^{ir} + R^{rd}} \tag{6}$$

$$z_m(k) = z_m^{ir}(k) + R^{ir}(R^{ir} + R^{rd})^{-1}(z_m^{rd}(k) - z_m^{ir}(k)) \tag{7}$$

The associated measurement noise covariance matrix (R) of the fused measurement vector [equation (6)] is computed as follows.

$$\frac{1}{R} = \frac{1}{R^{ir}} + \frac{1}{R^{rd}} \tag{8}$$

$$R = \left((R^{ir})^{-1} + (R^{rd})^{-1}\right)^{-1}$$

or

$$R = \frac{R^{ir}R^{rd}}{R^{ir}+R^{rd}} = \frac{R^{ir}R^{rd}}{R^{ir}+R^{rd}} - R^{ir} + R^{ir} \tag{9}$$

$$\left.\begin{aligned} R &= R^{ir} + \frac{R^{ir}R^{rd} - R^{ir}(R^{ir}+R^{rd})}{R^{ir}+R^{rd}} \\ R &= R^{ir} - R^{ir}(R^{ir}+R^{rd})^{-1}(R^{ir})^{T} \end{aligned}\right\} \tag{10}$$

## EXTENDED KALMAN FILTER

A general motion model used in discrete extended Kalman filter[1,5] for target tracking is

$$X(k) = FX(k-1) + Gw(k-1) \tag{11}$$

$$z(k) = h(X(k)) + v(k) \tag{12}$$

where $X(k)$ is the state vector; $F$, the state transition matrix; and $G$, the process noise gain matrix. The process noise $w(k)$ and the measurement noise $v(k)$ are zero-mean, mutually independent, white, Gaussian with covariance $Q$ and $R$, respectively. $z(k)$ is the measurement vector at time $k$ and $h(X(k))$ is a non-linear function of the states computed at time $k$.

Linear Kalman filter could be used for target tracking if the states and the measurements are in Cartesian coordinate system. Radar and IRST provide the measurements in a spherical coordinate system. In most cases the state vector could be estimated in Cartesian coordinate system. Equation (12) is non-linear and it needs to be linearized to fit into the Kalman filter framework entailing the use of extended Kalman filter (EKF).

### Time Propagation

The state and state covariance matrix at time $(k-1)$ are predicted to time $k$ as follows:

$$\left.\begin{aligned} \tilde{X}(k+1|k) &= F\hat{X}(k|k) \\ \tilde{P}(k+1|k) &= F\hat{P}(k|k)F^{T} + GQG^{T} \end{aligned}\right\} \tag{13}$$

where $\hat{X}$ is the estimated state vector; $\hat{P}$, the estimated state covariance matrix; $\tilde{X}$, the predicted state; and $\tilde{P}$, the predicted state covariance matrix.

### Measurement Update

Innovation

$$e = z_m(k+1) - \tilde{z}(k+1|k) \tag{14}$$

Innovation covariance

$$S = H(k)\tilde{P}(k+1|k)H(k)^{T} + R \tag{15}$$

where $\tilde{z}(k+1|k)$ is the predicted measurement; and $H(k)$, the linearized measurement matrix. The measurement update part consists of the following equations.

Filter gain

$$K = \tilde{P}(k+1|k)H(k)^{T}S^{-1} \tag{16}$$

Updated state

$$\hat{X}(k+1|k+1) = \tilde{X}(k+1|k) + Ke \tag{17}$$

Updated state covariance

$$\hat{P}(k+1|k+1) = [I - KH(k)]\tilde{P}(k+1|k) \tag{18}$$

### Predicted Measurement and Linearized Measurement Matrix

Partial derivative method is used to compute the linearized measurement matrix. Consider the state vector consisting of position, velocity and acceleration components in $x$-, $y$- and $z$-directions as

$$X = \begin{bmatrix} x & \dot{x} & \ddot{x} & y & \dot{y} & \ddot{y} & z & \dot{z} & \ddot{z} \end{bmatrix}^{T} \tag{19}$$

The predicted state is in the form

$$\begin{bmatrix} \tilde{x} & \dot{\tilde{x}} & \ddot{\tilde{x}} & \tilde{y} & \dot{\tilde{y}} & \ddot{\tilde{y}} & \tilde{z} & \dot{\tilde{z}} & \ddot{\tilde{z}} \end{bmatrix}^{T} = \tilde{X}(k+1|k) \tag{20}$$

The predicted measurement of fusion1 is

$$\tilde{z}(k+1|k) = h[\tilde{X}(k+1|k)] = \begin{bmatrix} \tilde{\theta} & \tilde{\varphi} & \tilde{\theta} & \tilde{\varphi} & \tilde{r} \end{bmatrix}^{T} \tag{21}$$

The predicted measurement of fusion2 is

$$\tilde{z}(k+1|k) = h[\tilde{X}(k+1|k)] = \begin{bmatrix} \tilde{\theta} & \tilde{\varphi} & \tilde{r} \end{bmatrix}^{T} \tag{22}$$

Components in the predicted measurement are computed

from the predicted state vector given in equation (20).

$$\left.\begin{aligned}\tilde{\theta} &= \tan^{-1}\left(\frac{\tilde{y}}{\tilde{x}}\right)\\ \tilde{\varphi} &= \tan\left(\frac{\tilde{z}}{\sqrt{\tilde{x}^2+\tilde{y}^2}}\right)\\ \tilde{r} &= \sqrt{\tilde{x}^2+\tilde{y}^2+\tilde{z}^2}\end{aligned}\right\} \quad (23)$$

*Finite Difference Method*

Calculation of linearized measurement matrix can be accomplished by the finite difference method. This method is generalized and flexible[2,6].

$$H(k) = H_{ij} = \left.\frac{\partial h_i}{\partial x_j}\right|_{x=\tilde{X}(k|k-1)} = \frac{h_i(x_j+\Delta x_j)-h_i(x_j)}{\Delta x_j} \quad (24)$$

where $i$ is 1,2,..., length of the measurement vector and $j$, 1,2,..., length of the state vector and $\Delta x_j$, the perturbation step size.

For small perturbation $\Delta x$ in each of the unknown variables, the perturbed value $h_i(x_j + \Delta x_j)$ is computed. The corresponding elements of $H_{ij}$ are given by the finite difference in the function [equation (24)] to changes in that state. In general, a perturbation step size of $10^{-7}$ is considered to be adequate.

## RESULTS AND DISCUSSION

The tracking algorithm using MVF1 and MVF2 is evaluated using some numerical simulated data.

### Numerical Simulation

Ground truth target trajectory with position, velocity and acceleration components in each of the three Cartesian coordinates $x$, $y$ and $z$-axis using the three-dof kinematic model are simulated to test the performance of the algorithms. The following parameters are considered in the simulation.

Sampling interval $T$, s : 0.25

Process noise variance $\sigma^2_w$ : 1e-6

Measurement noise variance :

| Sensor | Azimuth, rad | Elevation, rad | Range, m |
|---|---|---|---|
| IRST | 1e-6 | 1e-6 | – |
| Radar | 1e-4 | 1e-4 | 10 |

Duration of simulation, s : 125

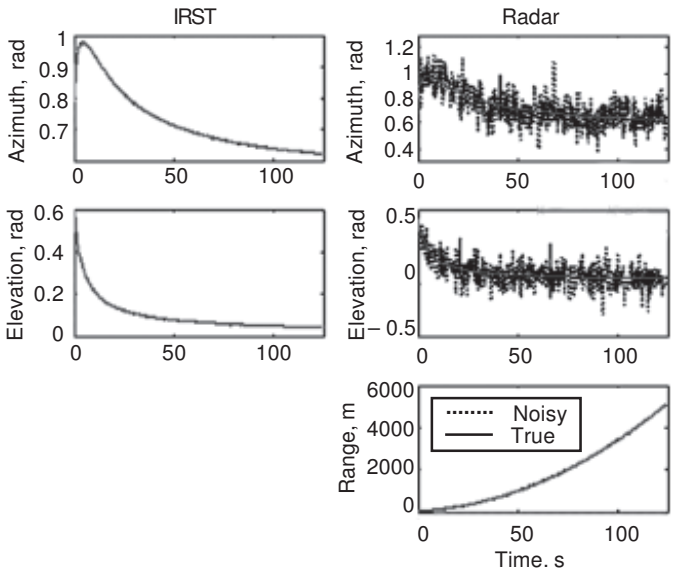


**Figure 2 True and noisy measurements of IRST and radar**

The simulated true and noisy measurements of radar (right half) and imaging (left half) sensors are shown in Figure 2.

Initial state vector is

$$X = [x \;\; \dot{x} \;\; \ddot{x} \;\; y \;\; \dot{y} \;\; \ddot{y} \;\; z \;\; \dot{z} \;\; \ddot{z}]^T$$
$$= [10 \;\; 2 \;\; 0.5 \;\; 10 \;\; 5 \;\; 0.3 \;\; 10 \;\; 1 \;\; 0.01]^T$$

The initial state vector to initialize the tracking filter is

$$\hat{X}_0 = 0.9 X_t \quad (25)$$

where $\hat{X}_0$ is the initial estimated state vector at scan number one; and $X_t$, the true state vector at scan number one.

The initial state error covariance matrix to initialize the tracking filter is

$$\hat{P}_0 = \text{diag}\left[(X_t - \hat{X}_0)^2\right] \quad (26)$$

The filter performance is checked by computing[7] the following:

The percentage fit error (PFE) in $x$-, $y$- and $z$-positions

$$\text{PFE}x = 100\,\frac{\text{norm}(x-\hat{x})}{\text{norm}(x)},$$

similarly for $y$- and $z$-positions (27)

Root mean square error in position

$$\text{RMSPE} = \sqrt{\frac{1}{N}\sum_{i=1}^{N}\frac{(x_i-\hat{x}_i)^2+(y_i-\hat{y}_i)^2+(z_i-\hat{z}_i)^2}{3}} \quad (28)$$

Root sum square error in position

$$\text{PSSPE} = \sqrt{(x-\hat{x})^2 + (y-\hat{y})^2 + (z-\hat{z})^2} \quad (29)$$

Absolute error in (AE) *x*-, *y*- and *z*-positions

$$\text{AE}_x(i) = \left|x(i) - \hat{x}(i)\right| \quad i = 1,2,\ldots,N,$$

similarly for *y*- and *z*-positions (30)

Mean absolute error in *x*-, *y*- and *z*-positions

$$\text{MAE}_x = \frac{1}{N}\sum_{i=1}^{N}\left|x(i) - \hat{x}(i)\right|,$$

similarly for *y*- and *z*-positions (31)

State error $(X - \hat{X})$ with theoretical bounds of $\pm 2\sqrt{\hat{P}}$ (32)

Innovation sequence $\left(z_m(k) - \tilde{z}(k|\,k-1)\right)$ with theoretical bounds of $\pm 2\sqrt{S}$ (33)

Normalized estimation error square $\left(X - \hat{X}\right)P^{-1}\left(X - \hat{X}\right)^T$ with theoretical bounds (34)

The lower bound is $\frac{\chi^{-1}(0.025, p)}{N_{MCS}}$ (34(a))

The upper bound is $\frac{\chi^{-1}(0.975, p)}{N_{MCS}}$ (34(b))

where degree of freedom $p$ is $N_X N_{MCS}$; $N_X$ is the number of elements in the state vector; $N_{MCS}$, number of Monte Carlo Simulations; and $\chi$, the chi-square operator.

Normalized innovation square $\vartheta S^{-1}\vartheta^T$ with theoretical bounds. (35)

The computation of bounds is similar to equations (34(a)) and (34(b)), except $p = N_Z N_{MCS}$, where $N_Z$, the number of elements in the measurement vector.

The root sum square errors in position (RSSPE), velocity (RSSVE) and accelerations (RSSAE) are shown in Figure 3. It is observed that the errors are small and settled down after a filter learns the dynamics. It is also observed that both the fusion algorithms show the similar performance.

Absolute errors in *x*-, *y*- and *z*-positions are shown in Figure 4. It is observed that the errors are small and both the fusion methods show similar results. Similar observation is seen in *x*-, *y*- and *z*-velocities and accelerations.

The normalized estimation error square (NEES) and

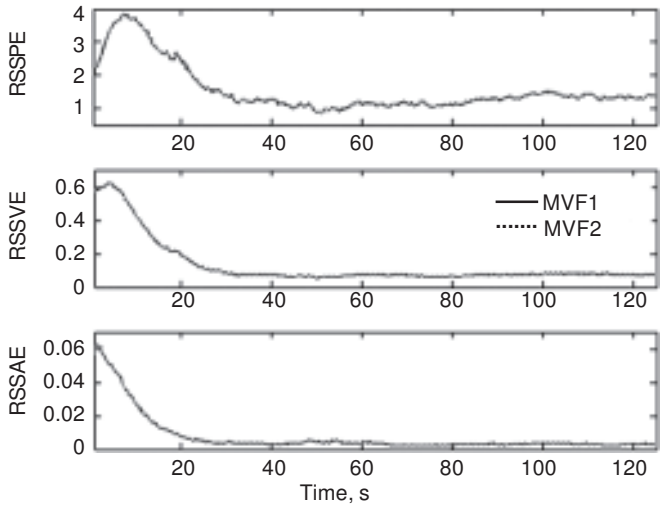


**Figure 3 Root sum square errors in position, velocity and acceleration**

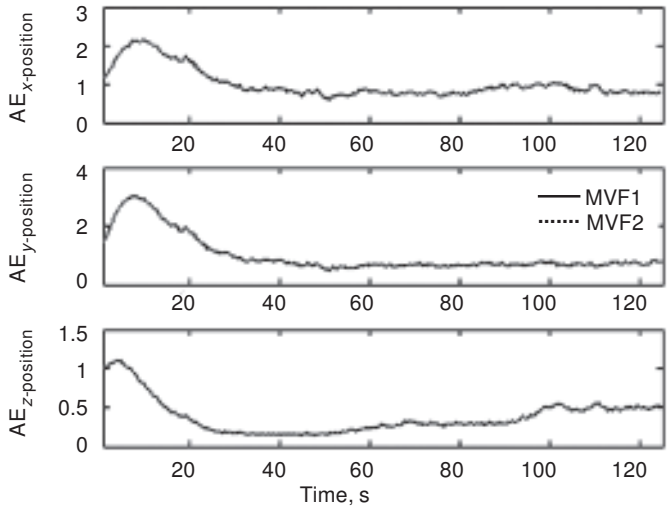


**Figure 4 Absolute error in *x*-, *y*- and *z*-positions**

normalized innovation square (NIS) are shown in Figure 5(a) and Figure 5(b), respectively. One can notice that NEES is outside the bounds and NIS is within the bounds. This indicates that compared to the filter calculated covariance, the state estimation errors are inadmissibly large. Thus, the filter is inconsistency in this case. It is concluded that large number of Monte Carlo simulations is required for consistency check to reach the meaningful result that is statistically stable.

The state errors in *x*-, *y*- and *z*-accelerations with theoretical bounds is shown in Figure 6. It is observed that all these errors are within the bounds show the filter robustness. Similarly, the state errors in *x*-, *y*- and *z*-positions and velocities are within the theoretical bounds. The innovation sequence with theoretical bounds is shown in Figure 7. It is observed that the innovation sequence is within the bonds that shows filter robustness.

The percentage fit error in *x*-, *y*- and *z*-positions, velocities and accelerations are given in Table 1. These values are

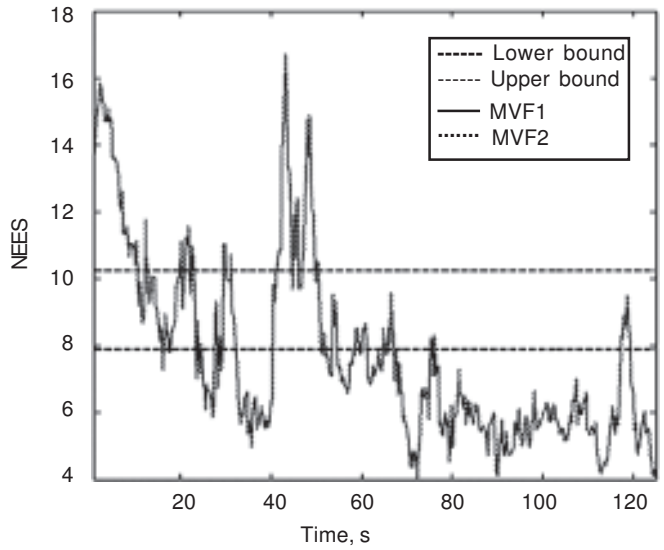


**Figure 5(a) Normalized estimation error square**

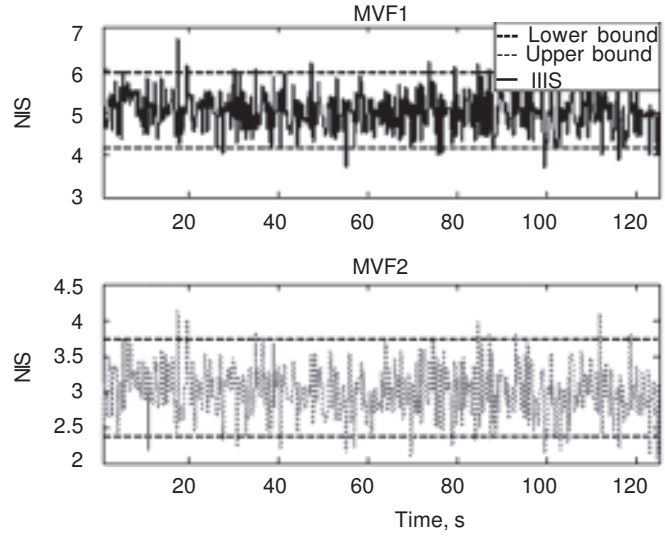


**Figure 5(b) Normalized innovation square**

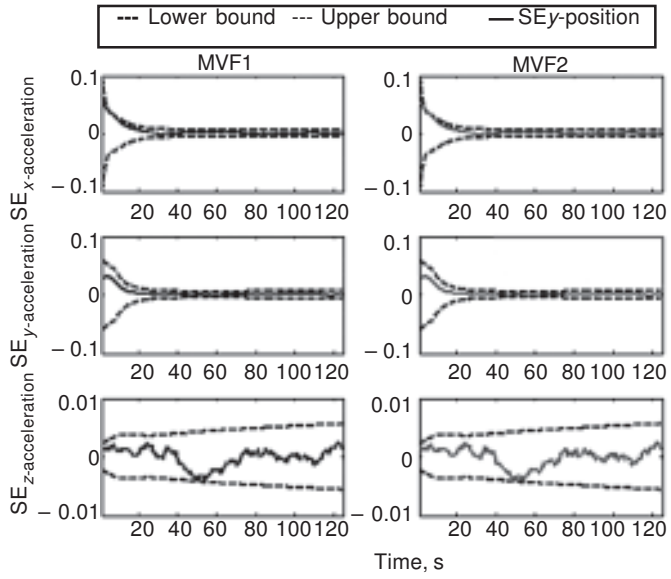


**Figure 6 State error in *x*-, *y*- and *z*-accelerations with theoretical bounds**

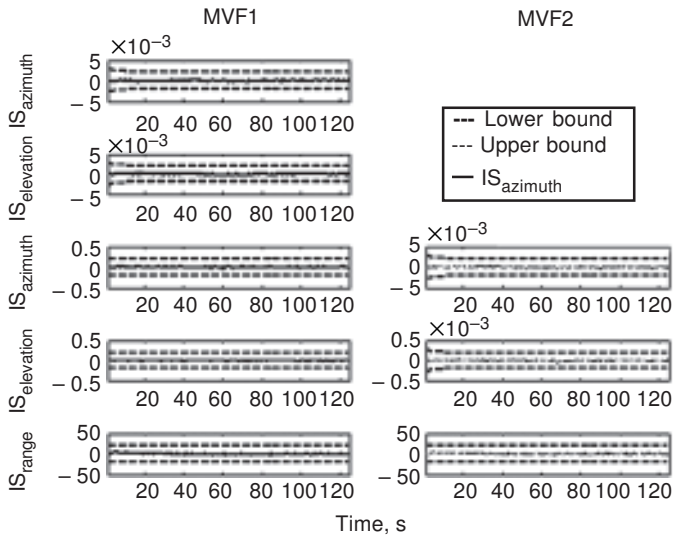


**Figure 7 Innovation sequence with theoretical bounds**

**Table 1 PFE in *x*-, *y*- and *z*-positions, velocities and accelerations**

| | PFE$x$ | PFE$y$ | PFE$z$ | PFE$\dot{x}$ | PFE$\dot{y}$ | PFE$\dot{z}$ | PFE$\ddot{x}$ | PFE$\ddot{y}$ | PFE$\ddot{z}$ |
|---|---|---|---|---|---|---|---|---|---|
| MVF1 | 0.65 | 0.096 | 0.436 | 0.319 | 0.603 | 2.319 | 2.435 | 2.913 | 18.316 |
| MVF2 | 0.65 | 0.096 | 0.436 | 0.319 | 0.603 | 2.319 | 2.435 | 2.913 | 18.316 |

within the limits. The mean absolute error in *x*-, *y*- and *z*-positions, velocities and accelerations are shown in Table 2. Root mean square error position (RMSPE), velocity (RMSVE) and acceleration (RMSAE), mean normalized estimation error (MNEES) and mean normalized innovation square (MNIS) are shown in Table 3. The MNEES is not equal to the length of the state vector. This indicates that filter is not consistency in this case. The MNIS is equal to the length of the measurement vector. It is concluded that large number of Monte Carlo simulations is required for consistency check to reach the meaningful conclusion. From Figures 3 to 7 and Tables 1 to 3, it is observed that both fusion methods are performed alike.

## PROOF TO SHOW MVF1 AND MVF2 FUNCTIONAL SIMILARITY

It is sufficient to check whether the terms $K(k)H(k)$ and $K(k)z_m(k)$ in MLF1 are functionally equivalent to those terms in MLF2, in order to demonstrate the functional equivalence of the two measurement fusion methods[8]. Figure 8 shows some of the elements in the product of $K(k)H(k)$. Figure 9

**Table 2 MAE in *x*-, *y*- and *z*-positions, velocities and accelerations**

| | MAE$x$ | MAE$y$ | MAE$z$ | MAE$\dot{x}$ | MAE$\dot{y}$ | MAE$\dot{z}$ | MAE$\ddot{x}$ | MAE$\ddot{y}$ | MAE$\ddot{z}$ |
|---|---|---|---|---|---|---|---|---|---|
| MVF1 | 1.004 | 1.005 | 0.379 | 0.078 | 0.089 | 0.029 | 0.005 | 0.004 | 0.001 |
| MVF2 | 1.004 | 1.005 | 0.379 | 0.078 | 0.089 | 0.029 | 0.005 | 0.004 | 0.001 |

**Table 3 Root mean square position, velocity and acceleration**

| | RMSPE | RMSVE | RMSAE | MNEES | MNIS |
|---|---|---|---|---|---|
| MVF1 | 1.101 | 0.117 | 0.009 | 7.7 | 4.978 |
| MVF2 | 1.101 | 0.117 | 0.009 | 7.7 | 2.986 |

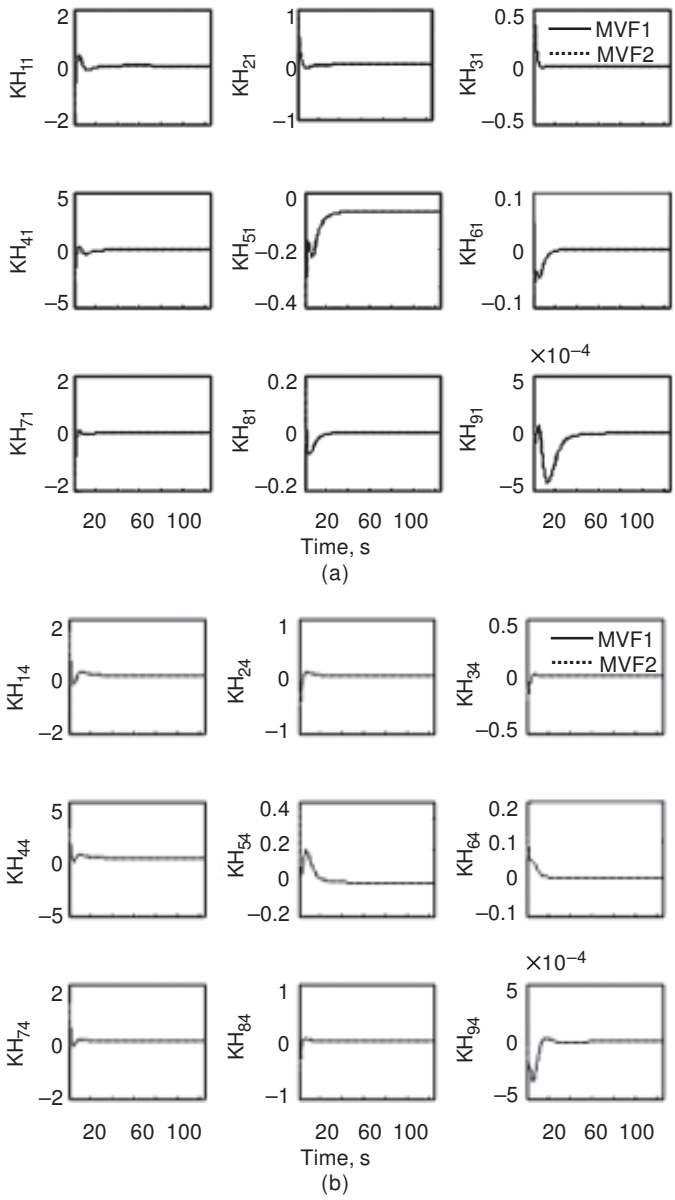


**Figure 8 Elements of KH**

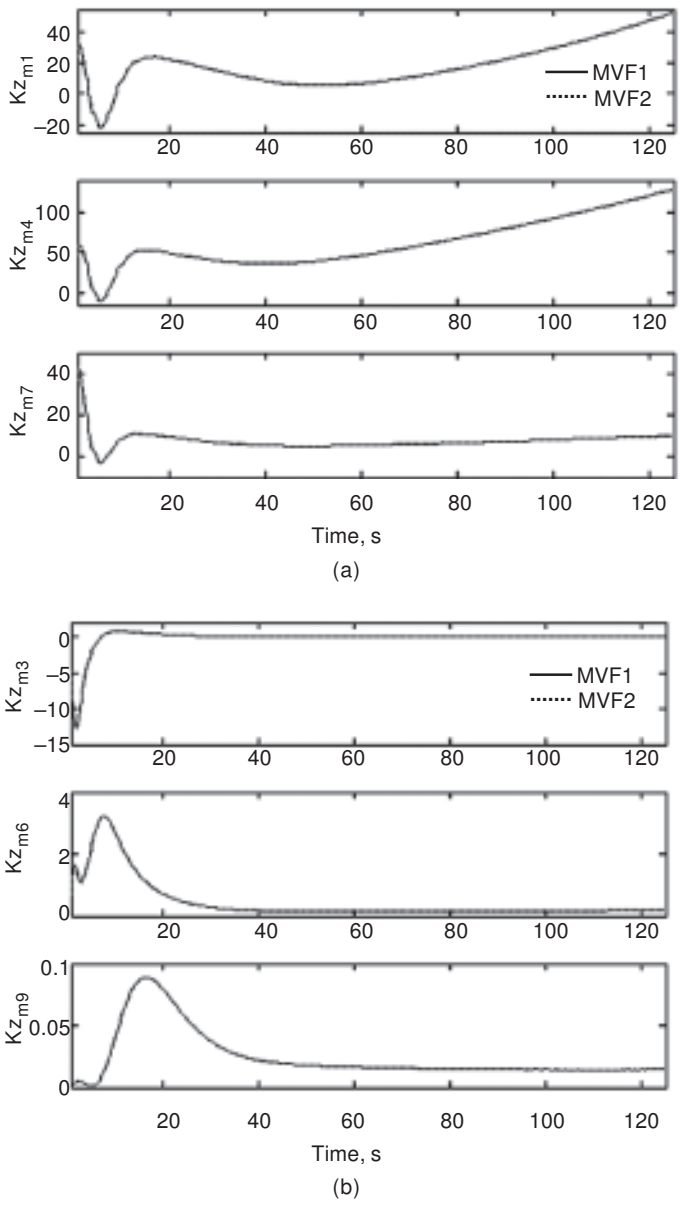


**Figure 9 Elements of $K_{zm}$**

shows the elements in the product of $K(k)z_m(k)$. It is observed that both fusion methods are alike. From the Figure 8 and Figure 9, it is concluded that both MVF1 and MVF2 are functionally equivalent.

## CONCLUSION

Two different types of measurement fusion methods for fusing IRST and radar measurements to track a target in 3D Cartesian coordinates have been evaluated. Performance evaluation metrics were provided to evaluate the tracking algorithm. It was observed that both fusion algorithms are performed alike. Proof was provided to show that both methods are functionally similar.

## REFERENCES

1. S Blackman and R Popoli. 'Design and Analysis of Modern Tracking Systems'. *Artech House*, London, 1999.

2. V P S Naidu and J R Raol. 'Fusion of Radar and Infrared Search and Track Data using Kalman Filter'. *NAL PD FC 0517*, 2005.

3. D L Hall and S A H McMullen. 'Mathematical Techniques in Multisensor Data Fusion'. Second Edition, *Artech House*, London, 2004.

4. J N Sanders-Reed. 'Error Propagation in Two-sensor 3D Position Estimation'. *Opt Eng*, vol 40, no 4, April 2001.

5. Y Bar-Shalom and X Li. 'Estimation and Tracking: Principles, Techniques, and Softwares'. *Artech House*, London, 1993.

6. G Girija and Z Christoph. 'Flight Path Reconstruction for Sensor Failure Detection and Health Monitoring'. *NAL PD FC 0418*, 2004.

7. V P S Naidu, G Girija and J R Raol. 'Data Association and Fusion Algorithms for Tracking in Presence of Measurement Loss'. *Journal of The Institute of Engineers* (*India*), vol 86, AS/1, May 2005, p 17.

8. C Harris, A Bailey and T Dodd. 'Multisensor Data Fusion in Defence and Aerospace'. *Journal of Aero Society*, vol 162, no 1015, 1998, p 229.